PAPER

Check for updates

Magnetic interactions controlled by light in the family of Fe(II)–M(IV) (M = Mo, W, Nb) hybrid organic–inorganic frameworks†

Michał Magott, [ID] *[a] Magdalena Ceglarska, [ID] [b] Michał Rams, [ID] [b]
Barbara Sieklucka [ID] [a] and Dawid Pinkowicz [ID] [a]

Three new hybrid organic–inorganic frameworks employing octacyanidometallates and 4,4′-bypyridine dioxide (4,4′-bpdo) as bridging molecules were prepared and characterized. The three-dimensional coordination frameworks $\{[Fe^{II}(\mu\text{-}4,4'\text{-bpdo})(H_2O)_2]_2[M^{IV}(CN)_8]\cdot9H_2O\}_n$ (**Fe$_2$Mo**, **Fe$_2$W** and **Fe$_2$Nb**; M = Mo, W and Nb) are composed of cyanido-bridged chains, which are interconnected by the organic linkers. Magnetic measurements for **Fe$_2$Nb** show a two-step transition to the antiferromagnetic state, which results from the cooperation of antiferromagnetic intra- and inter-chain interactions. **Fe$_2$Mo** and **Fe$_2$W**, on the other hand, behave as paramagnets at 2 K because of the diamagnetic character of the corresponding octacyanidometallate(IV) building units. However, after 450 nm light irradiation they show transition to the metastable high spin Mo^{IV} or W^{IV} states, respectively, with distinct ferromagnetic intrachain spin interactions, as opposed to the antiferromagnetic ones observed in the **Fe$_2$Nb** framework.

Introduction

One-dimensional coordination polymers play a central role in the field of molecular magnetism, which emerged with studies of chain assemblies based on radical molecules[1,2] and later expanded with the discovery of Single Chain Magnets (SCMs),[3–8] one-dimensional analogues of Single Molecule Magnets (SMMs).[9] These materials are expected to enable high-density information storage in future devices, due to their molecular character.[10–12] However, in order to achieve functional control over these units, the appropriate chemical tools need to be developed. In the case of SMMs, ordered molecular architectures were prepared by embedding such molecules in metal–organic frameworks.[13–16] Among SCMs, a similar strategy was employed for cobalt(II) compounds[17] and only a few examples of iron(II) chains 'trapped' inside higher dimensional frameworks were described so far.[18–20] The alternative approach to future magnetic memory devices is based on photo-switchable assemblies, where multiple magnetic states may be addressed with light.[21–24] Introduction of

suitable building units into 1-D coordination polymers led to the discovery of photo-switchable chain compounds showing light-induced changes in the paramagnetic properties[25–27] and in some cases slow magnetic relaxation triggered by UV-vis irradiation.[28–32]

Herein we demonstrate three analogous cyanido-bridged chains based on iron(II) and three different octacyanidometallates(IV), which are organized into a three-dimensional (3D) architecture by an organic linker molecule – 4,4′-bipyridine dioxide (4,4′-bpdo): $\{[Fe^{II}(\mu\text{-}4,4'\text{-bpdo})(H_2O)_2]_2[M^{IV}(CN)_8]\cdot 9H_2O\}_n$ (M = Mo, W and Nb; **Fe$_2$Mo**, **Fe$_2$W** and **Fe$_2$Nb**). In the case of **Fe$_2$Nb**, the intrachain antiferromagnetic (AF) exchange interactions mediated by the cyanido ligands between the Nb^{IV} and Fe^{II} centers, and interactions transmitted through the long 4,4′-bpdo molecules linking Fe^{II} centres and through space, cause a transition to the AF phase below 5.6 K. On the other hand, for compounds comprising diamagnetic octacyanidomolybdate(IV) (**Fe$_2$Mo**) or octacyanidotungstate(IV) (**Fe$_2$W**), the irradiation by 450 nm light activates ferromagnetic intrachain interactions. To our knowledge, this is the first demonstration of the octacyanidometallate-centred photomagnetism in Fe^{II}–M(CN)$_8$ coordination polymers.

[a]Faculty of Chemistry, Jagiellonian University, Gronostajowa 2, 30-387 Kraków, Poland. E-mail: michal.magott@uj.edu.pl
[b]Jagiellonian University, Institute of Physics, Łojasiewicza 11, 30-348 Kraków, Poland

Experimental section

$K_4[Nb^{IV}(CN)_8]\cdot2H_2O$,[33] $K_4[Mo^{IV}(CN)_8]\cdot2H_2O$,[33] $K_4[W^{IV}(CN)_8]\cdot 2H_2O$[34] and 4,4′-bipyridine dioxide[35] (4,4′-bpdo) were obtained

according to published procedures. All other reagents were purchased from Sigma-Aldrich and used as supplied.

$\{[Fe^{II}(\mu\text{-}4,4'\text{-bpdo})(H_2O)_2]_2[M^{IV}(CN)_8]\cdot 9H_2O\}_n$ (Fe$_2$Mo for M = Mo, Fe$_2$W for M = W, and Fe$_2$Nb for M = Nb)

A solution of $Fe(NH_4)_2(SO_4)_2\cdot 6H_2O$ (0.084 mmol, 33 mg) and 4,4′-bypyridine dioxide hemihydrate (0.4 mmol, 80 mg) in 12 mL of water was dropwise added to a solution of the respective potassium octacyanidometallate(IV) (0.05 mmol, 25 mg for octacyanidomolybdate(IV) and octacyanidoniobate (IV), 28 mg for octacyanidotungstate(IV)) dissolved in 10 mL of water. After 24 hours needle-shaped crystals were collected by decantation. Typical yield in 10 repetitions: 15–20 mg (30–40% based on Fe). Sample purity was confirmed by powder X-ray diffraction (Fig. S1–3†) and elemental analysis. EA Found for **Fe$_2$Mo**: C 32.69, H 3.93, N 16.31; calculated for Fe$_2$MoC$_{28}$N$_{12}$O$_{17}$H$_{42}$: C 32.77, H 4.12, N 16.38. Found for **Fe$_2$W**: C 29.74, H 4.08, N 15.05; calculated for Fe$_2$WC$_{28}$N$_{12}$O$_{17}$H$_{42}$: C 30.18, H 3.80, N 15.08. Found for **Fe$_2$Nb**: C 32.95, H 3.88, N 16.52; calculated for Fe$_2$NbC$_{28}$N$_{12}$O$_{17}$H$_{42}$: C 32.83, H 4.14, N 16.43. The infrared spectra of the three compounds are demonstrated in the ESI (Fig. S4–6†).

Results and discussion

Crystal structures

The three coordination polymers **Fe$_2$Mo**, **Fe$_2$W** and **Fe$_2$Nb** are isomorphous and crystallize in a self-assembly process as needle-shaped crystals in $C2/c$ space group (Table S1† in the ESI†). Iron(II) cations are linked by octacyanidometallate(IV) anions to form vertex-sharing coordination chains (Fig. 1a). Within each chain, the $[M^{IV}(CN)_8]^{4-}$ moieties form four coordination bridges to four iron(II) centres, while the four remaining cyanido ligands are engaged in hydrogen bonds with crystallization water molecules. The coordination sphere of Fe(II) consists of two nitrogen atoms of the bridging CN$^-$ ligands, two oxygen atoms of 4,4′-bipyridine dioxide molecules in the *trans* geometry and is completed by two water molecules in the *cis* configuration (Fig. S7†). Organic linkers bridge iron(II) cations in the *anti*-configuration,[36] connecting inorganic {Fe^{II}–NC–M^{IV}} chains into a three-dimensional I^1O^2 organic–inorganic framework[37] depicted in Fig. 1b. In all three reported compounds, the octacyanidometallate moiety attains a dodecahedral geometry and the iron(II) centres exhibit a slightly distorted octahedral environment, as verified by the continuous symmetry measures using SHAPE software[38] (Table S2†). The coordination frameworks are stabilized by numerous hydrogen bonds between the water molecules, nitrogen atoms of terminal cyanides and oxygen atoms of 4,4′-bipyridine dioxide. Interestingly, there are also relatively short contacts between terminal cyanides and centroids of bpdo aromatic rings (Fig. S8†). The corresponding N3–centroid distances are 3.290 (3) Å for **Fe$_2$Mo** and **Fe$_2$W**, and 3.230(2) Å for **Fe$_2$Nb**. The difference of 0.06 Å may be explained by the elongation of the appropriate M^{IV}–CN bond from 2.160(3) Å to 2.255(3) Å upon

Fig. 1 Schematic representation of cyanido-bridged coordination chains along crystallographic *a* axis (a) and coordination layers formed by 4,4′-bpdo linker molecules along crystallographic *c* direction (b) in the structure of **Fe$_2$Mo**.

substitution of Mo/W with Nb or by a larger electron density at the N3 atom of the $[Nb^{IV}(CN)_8]$ moiety in **Fe$_2$Nb**. The presence of these structural motifs may indicate a significant role of anion–pi interactions in the self-assembly process, which was previously studied for other cyanidometallate-based assemblies with π-deficient molecules/ligands.[39,40]

Magnetic properties

Fe$_2$Mo and **Fe$_2$W** comprise paramagnetic iron(II) centres linked by diamagnetic octacyanidometallates(IV). At 250 K they show the χT product of 7.4 cm^3 K mol^{-1} (Fig. 2), indicating that both iron(II) cations are in the high spin state, as can be anticipated for the N$_2$O$_4$ coordination environment of Fe^{II} based on the structural data. Below 50 K, these compounds show a distinct decrease of χT, down to 2.0 cm^3 K mol^{-1} at 1.8 K for **Fe$_2$Mo** and 2.3 cm^3 K mol^{-1} at 1.8 K for **Fe$_2$W** due to the zero field splitting (zfs) effect and antiferromagnetic interactions

a)

b)

Fig. 2 Temperature dependence of χT at 0.1 T and magnetic field dependence of magnetization at 1.8 K (inset) recorded for **Fe$_2$Mo** (a) and **Fe$_2$W** (b). Green lines demonstrate the result of $\chi T(T)$ and $M(H)$ fitting.

between the Fe^{II} centres. The magnetization *versus* field curves recorded at 1.8 K reach at 7 T values 5.4 $N\beta$ and 5.7 $N\beta$ for **Fe$_2$Mo** and **Fe$_2$W**, respectively (Fig. 2, insets). These values are far from the saturation value of 8.8 $N\beta$ expected for two iron(II) ions with $g = 2.2$, and such behaviour is in line with zfs effect. Measured dependences were quantitatively analysed with the following Hamiltonian:

$$\hat{H} = \sum_n \left[-2J_{FeFe}\vec{S}_n \cdot \vec{S}_{n+1} + D(S_{nz}{}^2 - 2) + g_{Fe}\beta\vec{H}\vec{S}_n \right]$$

assuming that the iron(II) cations with $S = 2$, as linked by bpdo ligands, are AF coupled into chains. To facilitate calculations, a finite model of a ring comprising 4 such spins was used to fit simultaneously $\chi T(T)$ and $M(H)$ dependences using MAGPACK[41] based program. The best fit parameters J_{FeFe} (superexchange coupling constant) and D (zfs parameter) summarized in Table 1 are similar for both compounds. The reported J_{FeFe} values are in line with previous studies of systems bridged by the 4,4'-bpdo linker,[42,43] as well as D para-

Table 1 Parameters derived from simultaneous fitting of $\chi T(T)$ and $M(H)$ dependence for the paramagnetic frameworks **Fe$_2$Mo** and **Fe$_2$W**

Compound	g	D/cm^{-1}	J_{FeFe}/cm^{-1}
Fe$_2$Mo	2.22(3)	−10.1(1)	−0.073(5)
Fe$_2$W	2.22(2)	−10.0(1)	−0.069(3)

meters falling in the expected range for iron(II) systems.[44–47] Nonetheless, the obtained J and D should be treated rather as approximate values, as our model does not account for super-exchange interactions transferred by long [–NC–M^{IV}(CN)$_6$–CN–] linkers and dipole–dipole interactions between neighbouring iron(II) ions.

The peaks of specific heat (Fig. 3), observed at T_c = 1.20 K and 1.30 K for **Fe$_2$Mo** and **Fe$_2$W**, respectively, demonstrate the magnetic ordering of these compounds. The entropy change for **Fe$_2$Mo** is 5.71 J mol^{-1} K^{-1} from 0.5 to 5 K, which is very close to Rln 2 corresponding to ordering of a spin doublet system, such as the ground state S_z = ±2 doublet of Fe^{II} in **Fe$_2$Mo**. In both cases, over 60% of the entropy change is observed above T_c, in line with the dominant exchange within Fe-bpdo-Fe chains, and much weaker inter-chain inter-actions.[48] As aforementioned, the iron(II) cations in **Fe$_2$Mo** and **Fe$_2$W** are connected *via* diamagnetic octacyanidomolybdate(IV) and octacyanidotungstate(IV) linkers. For the **Fe$_2$Nb** analogue, the presence of the spin s = 1/2 of the octacyanidoniobate(IV), results in higher χT = 7.6 cm^3 K mol^{-1} at 250 K and most importantly, leads to the decrease of χT that starts already below 100 K, indicating antiferromagnetic exchange, J_{FeNb}, *via* Fe^{II}–NC–Nb^{IV} bridges (Fig. S9†). Upon further temperature decrease, the $\chi(T)$ measured in fields below 0.8 T reaches a maximum at T_{c2} = 5.6 K (Fig. 4a), and another inflection at T_{c1} = 3.7 K is observed, resulting in the even faster susceptibility decrease. The specific heat of **Fe$_2$Nb** (Fig. 3) shows a λ-shaped peak typical for 3D ordering at 5.50 K and also a small feature

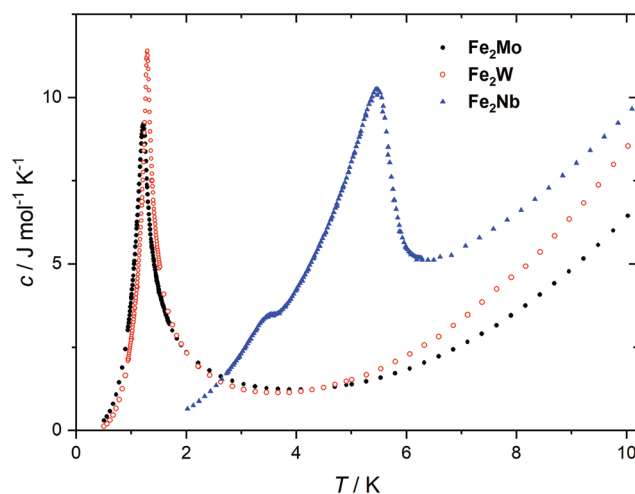**Fig. 3** Specific heat of **Fe$_2$Mo**, **Fe$_2$W** and **Fe$_2$Nb**, measured at zero magnetic field.

Fig. 4 Temperature dependence of χ for various magnetic fields (a) and magnetic field dependence of magnetization at various temperatures (b) recorded for **Fe$_2$Nb**. Solid lines are guides for an eye.

at 3.55 K. Zero-field cooled (zfc) and field cooled (fc) magnetization curves for **Fe$_2$Nb** show no divergence (Fig. S10†), there is no frequency dependence of AC magnetic signal (Fig. S11†) and magnetic hysteresis loop is not observed at 1.8 K (Fig. S12†). A two-step transition is also present in the magnetization field dependence (Fig. 4b). The first step is visible around $\mu_0 H_{c1} = 0.95$ T at 1.8 K, while a more subtle step starts around $\mu_0 H_{c2} = 3.8$ T (Fig. S13†). All these measurements consistently show that **Fe$_2$Nb** has an AF ground state magnetic structure, but there is also another ordered structure between T_{c1} and T_{c2}, that is also fully compensated AF at $H = 0$. An identification of involved metamagnetic processes can be inferred by comparison with **Fe$_2$Mo**, where at a field 0.5 T a similar step in $M(H)$ curve starts to form (Fig. 2a, inset). This suggests that the transition at H_{c1} in **Fe$_2$Nb** is caused by overcoming of J_{FeFe} interaction by external field, *i.e.* flipping spins of whole Fe$_2$Nb chains. The condition for such spin–flip: $-4zJ_{FeFe}S^2 = 2\beta H_{c1}(2g_{Fe}S - g_{Nb}s)$ takes into account $z = 4$ spin interaction paths J_{FeFe} per one Fe$_2$Nb unit, and effectively Ising-like exchange in the zfs ground state. This, for $S = 2$, $g_{Fe} = 2.2$ and $g_{Nb} = 2.0$, leads to $J_{FeFe} = -0.10$ cm^{-1}, slightly stronger than for **Fe$_2$Mo**.

A smaller $M(H)$ step at H_{c2} remains to be related to flipping of Nb spins when the field overcomes the J_{FeNb} interaction. A similar estimation as before leads to $J_{FeNb} = -0.24$ cm^{-1} using $-4zJ_{FeNb}Ss = 2\beta g_{Nb}H_{c2}s$ for $s = 1/2$ and $z = 4$.

Assuming similar zfs in **Fe$_2$Nb** as in **Fe$_2$Mo**, the excited zfs state of Fe(II) is above 30 cm^{-1}, which excludes its direct interfering with the ground magnetic state in the measured field range. However, still more complicated scenarios of magnetic structures sequence are possible, such as spin rearrangement, because the AF structure is expected to be non-collinear, due to presence of two different orientations of Fe(II) in the crystal lattice, and anisotropic zfs ground state of Fe(II).

Photomagnetic properties

Octacyanidomolybdate(IV) and octacyanidotungstate(IV) were demonstrated to behave as photomagnetic chromophores (intrinsic photomagnetic units).[27,49–52] As aforementioned, both $[Mo^{IV}(CN)_8]^{4-}$ and $[W^{IV}(CN)_8]^{4-}$ are characterized by diamagnetic $S = 0$ ground state, where d^2 electrons are paired on a single lowest lying orbital. However, after blue light irradiation Mo^{IV} and W^{IV} may be excited to the metastable $S = 1$ state, which in the case of K$_4$[Mo^{IV}(CN)$_8$]·2H$_2$O was demonstrated to arise from the photoinduced cyanide dissociation, yielding heptacyanidomolybdate(IV).[53] The initial diamagnetic state may be recovered by heating the sample above a certain temperature at which the thermal relaxation is very fast.

In order to test the possibility of a photomagnetic switching in **Fe$_2$Mo** and **Fe$_2$W**, the samples of both compounds were cooled to 10 K and subjected to 450 nm light irradiation. This irradiation wavelength was selected based on UV-vis spectra of **Fe$_2$Mo** and **Fe$_2$W** depicted in Fig. S14.† Both compounds show broad transition in 450–650 nm range. This band is associated with iron(II)–centred d–d transitions and the d–d transition of the $[Mo^{IV}(CN)_8]$ and $[W^{IV}(CN)_8]$ moieties, respectively.[27,53,54] After turning the light on, the sudden drop of the χT is observed (Fig. S15†), which is related to the heating of the samples by *ca.* 2 K due to the light absorption. Upon continued irradiation, the χT slowly increases as the octacyanidometallate(IV) moieties are gradually converted from the $S = 0$ to the photoexcited $S = 1$ state. However, even after prolonged irradiation (20 h and nearly 40 h for **Fe$_2$Mo** and **Fe$_2$W**, respectively) no saturation has been observed, indicating that the photo-conversion to the high-spin state could not be fully completed. Finally, turning the light off leads to the sudden increase of the χT, resulting from the sample temperature equilibration. For **Fe$_2$Mo**, a total increase of χT from 5.4 to 11.4 cm^3 K mol^{-1} is observed after 23 hours of 450 nm irradiation at 10 K, while in the case of **Fe$_2$W**, the χT product changes from 5.4 to 9.4 cm^3 K mol^{-1} as a result of 39 hours of light exposure. After turning the light off both compounds show no evolution of the magnetic signal (within 30 minutes). Therefore, both **Fe$_2$Mo** and **Fe$_2$W** clearly show light-induced transition to the metastable state with negligible relaxation at 10 K.

After light irradiation at 10 K both **Fe$_2$Mo** and **Fe$_2$W** were cooled to 2 K and magnetic field dependence of magnetization

was recorded (Fig. 5). In the case of **Fe₂W**, the magnetization after irradiation is higher in the whole 0–7 T magnetic field range, reaching 6.15 $N\beta$ as compared to 5.65 $N\beta$ at 7 T before irradiation. The $M(H)$ dependence with M values higher in the whole 0–7 T magnetic field range as compared with the "dark" initial state, indicates ferromagnetic superexchange interactions between the Fe^{II} and photo-induced $S = 1$ W^{IV} centres, as opposed to antiferromagnetic superexchange observed in **Fe₂Nb**. The $M(H)$ curve for **Fe₂Mo** also shows higher magnetization values after irradiation, with the value at saturation of 6.1 $N\beta$ at 7 T as compared to 5.5 $N\beta$ for the initial "dark" state. However, in the 2–3.5 T magnetic field range there is a distinct overlap of the experimental points recorded before and after light irradiation. This might result from the unaccounted anisotropy of the photo-induced $S = 1$ Mo^{IV} centres[53] and/or antiferromagnetic interactions between the photo-induced chain fragments in **Fe₂Mo**, which seem to be responsible for the long-range antiferromagnetic ordering in **Fe₂Nb**.

Measurements of magnetization field dependence after blue light irradiation were followed by $\chi T(T)$ measurements at 0.1 T in 2–150 K range, which are depicted in Fig. 6 (above 150 K the signal of the sample is almost completely obscured by the diamagnetism of the sample holder, hence, the measurements were stopped at this temperature). The χT for the irradiated states of both compounds shows a significant increase upon heating starting from 2 K and reaching the maximum value of 11.1 cm³ K mol⁻¹ at 11 K for **Fe₂Mo** and 9.5 cm³ K mol⁻¹ at 15 K for **Fe₂W**. The appearance of the maximum indicates ferromagnetic intra-chain interactions via cyanido bridges that compete with the antiferromagnetic inter-chain ones via 4,4′-bpdo linkers. Further heating leads to the gradual decrease of χT for both compounds, at 150 K reaching 8.7 and 7.6 cm³ K mol⁻¹ for **Fe₂Mo** and **Fe₂W**, respectively. Both values are noticeably higher than 7.3 cm³ K mol⁻¹ observed before irradiation, indicating that at 150 K the thermal relaxation is still slow and the initial state is not fully

Fig. 5 Magnetic field dependence of magnetization at 2.0 K recorded for **Fe₂Mo** (a) and **Fe₂W** (b) before light irradiation (black points) and after 450 nm light irradiation (red points).
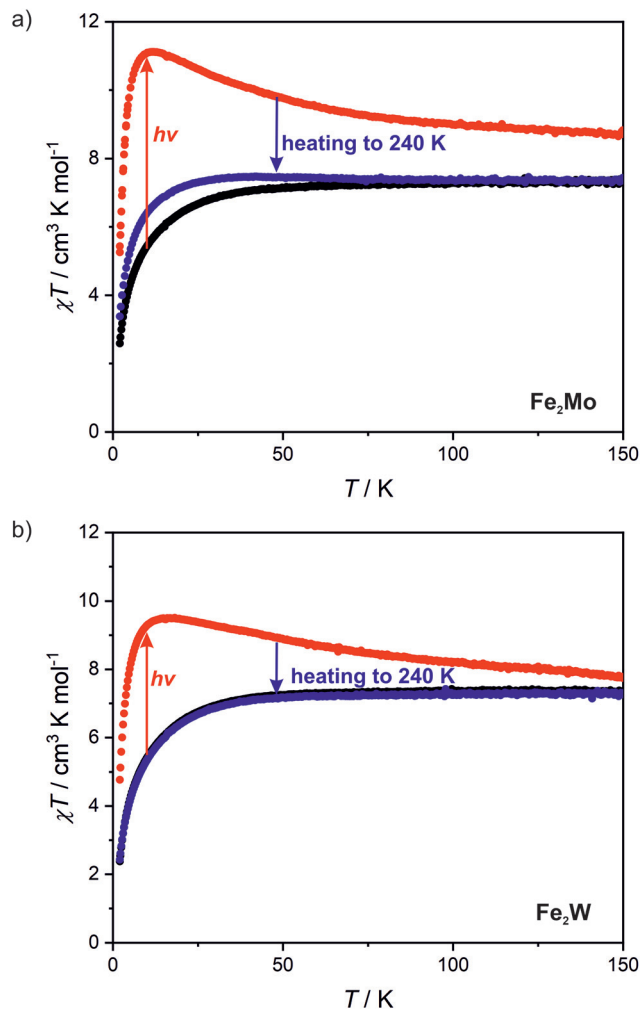
Fig. 6 Temperature dependence of χT at 0.1 T recorded for **Fe₂Mo** (a) and **Fe₂W** (b) before light irradiation (black points), after 450 nm light irradiation (red points) and after thermal relaxation at 240 K (blue points).

restored. The analysis of the slope of the χT curves after irradiation presented in Fig. 6 suggests that **Fe₂W** undergoes thermal relaxation more readily than **Fe₂Mo**. In order to enforce complete restoration of the initial state, both compounds were heated to 240 K and kept at this temperature for 1 hour (higher temperatures were avoided to prevent dehydration of the compounds). The $\chi T(T)$ curve obtained for **Fe₂Mo** after thermal relaxation still does not overlap perfectly with the initial one below 80 K, indicating the presence of the "remnant" paramagnetic molybdenum centres still present after the irradiation. The $\chi T(T)$ curve recorded after the thermal relaxation for **Fe₂W**, on the other hand, shows perfect agreement with that recorded before the irradiation experiment. This indicates that octacyanidotungstate(ɪᴠ) either shows better reversibility of the photo-induced transition or undergoes thermal relaxation in lower temperature range than the octacyanidomolybdate(ɪᴠ), which is in line with similar previous observations for $\{[Mn^{II}(imH)]_2[M^{IV}(CN)_8]\}_n$ (M = Mo, W) compounds.[55,56]

Conclusions

We have designed, obtained and characterized three new hybrid organic–inorganic I^1O^2 coordination frameworks composed of inorganic cyanido-bridged chains interconnected by organic linker molecules to form a 3D coordination architecture. In the case of octacyanidomolybdate(ɪᴠ)- and octacyanidotungstate(ɪᴠ)-based **Fe₂Mo** and **Fe₂W** compounds, the iron(ɪɪ) centres are only weakly interacting through the 4,4′-bpdo ligands and their magnetic behaviour is governed mainly by significant zero-field splitting effects associated with Fe^{II}. In the case of **Fe₂Nb**, the magnetic interactions between spins of iron(ɪɪ) and niobium(ɪᴠ) transmitted through the short CN-bridges lead to the emergence of an antiferromagnetic ordering below 5.6 K with an additional magnetic transition. The complex magnetic behaviour of **Fe₂Nb** results most probably from the hybrid organic–inorganic architecture of this compound with the antiferromagnetic Fe^{II}–NC–Nb^{IV} interactions giving rise to the long-range ferrimagnetic correlation along the inorganic chains, which are further antiferromagnetically coupled to yield a complex 3D magnetic structure. **Fe₂Mo** and **Fe₂W**, on the other hand, show photomagnetic behaviour. The light-induced activation of high spin Mo^{IV} or W^{IV} centres, respectively, leads to the appearance of ferromagnetic Fe^{II}–NC–Mo^{IV}/W^{IV} superexchange interactions. Therefore, by the appropriate combination of the chemical design and physical stimuli (light and temperature) one can achieve paramagnetic (**Fe₂Mo** and **Fe₂W** before irradiation), antiferromagnetic (**Fe₂Nb**) and ferromagnetically-coupled states (**Fe₂Mo** and **Fe₂W** after irradiation) within the $\{[Fe^{II}(\mu\text{-}4,4'\text{-bpdo})(H_2O)_2]_2[M^{IV}(CN)_8]\cdot 9H_2O\}_n$ (M = Nb, Mo, W) family of compounds. Moreover, when the photo-irradiated **Fe₂Mo** and **Fe₂W** are heated to 240 K in order to reverse the photo-induced changes, the ground diamagnetic state of the octacyanidometallate(ɪᴠ) chromophores can be fully recovered only for **Fe₂W**.

This is in line with our previous studies of Mo^{IV}/W^{IV} photomagnetic assemblies[55,56] and may indicate better reversibility of the photomagnetic effects in octacyanidotungstate(ɪᴠ)-based compounds.

Author contributions

M. Magott: conceptualization, investigation, writing – original draft, writing – review & editing; M. Ceglarska: investigation, funding acquisition; M. Rams: investigation, writing – review & editing; B. Sieklucka: funding acquisition, supervision, writing – review & editing; D. Pinkowicz: conceptualization, funding acquisition, project administration, supervision, writing – review & editing. All authors reviewed and agreed to the final version of the manuscript.

Conflicts of interest

There are no conflicts to declare.

Acknowledgements

Notes and references

1 G. A. Candela, L. J. Swartzendruber, J. S. Miller and M. J. Rice, *J. Am. Chem. Soc.*, 1979, **101**, 2755–2756.

2 A. H. Reis, L. D. Preston, J. M. Williams, S. W. Peterson, G. A. Candela, L. J. Swartzendruber and J. S. Miller, *J. Am. Chem. Soc.*, 1979, **101**, 2756–2758.

3 A. Caneschi, D. Gatteschi, N. Lalioti, C. Sangregorio, R. Sessoli, G. Venturi, A. Vindigni, A. Rettori, M. G. Pini and M. A. Novak, *Angew. Chem., Int. Ed.*, 2001, **40**, 1760–1763.

4 R. Clérac, H. Miyasaka, M. Yamashita and C. Coulon, *J. Am. Chem. Soc.*, 2002, **124**, 12837–12844.

5 R. Lescouëzec, J. Vaissermann, C. Ruiz-Pérez, F. Lloret, R. Carrasco, M. Julve, M. Verdaguer, Y. Dromzee, D. Gatteschi and W. Wernsdorfer, *Angew. Chem., Int. Ed.*, 2003, **42**, 1483–1486.

6 M. Ferbinteanu, H. Miyasaka, W. Wernsdorfer, K. Nakata, K.-i. Sugiura, M. Yamashita, C. Coulon and R. Clérac, *J. Am. Chem. Soc.*, 2005, **127**, 3090–3099.

7 H. Miyasaka, M. Julve, M. Yamashita and R. Clérac, *Inorg. Chem.*, 2009, **48**, 3420–3437.

8 R.-M. Wei, F. Cao, J. Li, L. Yang, Y. Han, X.-L. Zhang, Z. Zhang, X.-Y. Wang and Y. Song, *Sci. Rep.*, 2016, **6**, 24372.

9 S. M. J. Aubin, M. W. Wemple, D. M. Adams, H.-L. Tsai, G. Christou and D. N. Hendrickson, *J. Am. Chem. Soc.*, 1996, **118**, 7746–7754.

10 R. Sessoli, D. Gatteschi, A. Caneschi and M. A. Novak, *Nature*, 1993, **365**, 141–143.

11 L. Bogani, A. Vindigni, R. Sessoli and D. Gatteschi, *J. Mater. Chem.*, 2008, **18**, 4750–4758.

12 J. M. Frost, K. L. M. Harriman and M. Murugesu, *Chem. Sci.*, 2016, **7**, 2470–2491.

13 G. Huang, G. Fernandez-Garcia, I. Badiane, M. Camarra, S. Freslon, O. Guillou, C. Daiguebonne, F. Totti, O. Cador, T. Guizouarn, B. Le Guennic and K. Bernot, *Chem. – Eur. J.*, 2018, **24**, 6983–6991.

14 L. H. G. Kalinke, D. Cangussu, M. Mon, R. Bruno, E. Tiburcio, F. Lloret, D. Armentano, E. Pardo and J. Ferrando-Soria, *Inorg. Chem.*, 2019, **58**, 14498–14506.

15 D. Aulakh, L. Liu, J. R. Varghese, H. Xie, T. Islamoglu, K. Duell, C.-W. Kung, C.-E. Hsiung, Y. Zhang, R. J. Drout, O. K. Farha, K. R. Dunbar, Y. Han and M. Wriedt, *J. Am. Chem. Soc.*, 2019, **141**, 2997–3005.

16 S. Chorazy, R. Podgajny, W. Nitek, M. Rams, S.-i. Ohkoshi and B. Sieklucka, *Cryst. Growth Des.*, 2013, **13**, 3036–3045.

17 M. Wang, X. Gou, W. Shi and P. Cheng, *Chem. Commun.*, 2019, **55**, 11000–11012.

18 Y.-Z. Zheng, W. Xue, M.-L. Tong, X.-M. Chen, F. Grandjean and G. J. Long, *Inorg. Chem.*, 2008, **47**, 4077–4087.

19 Y.-Q. Wang, Q. Yue, Y. Qi, K. Wang, Q. Sun and E.-Q. Gao, *Inorg. Chem.*, 2013, **52**, 4259–4268.

20 J. Chen, Y. Sekine, Y. Komatsumaru, S. Hayami and H. Miyasaka, *Angew. Chem., Int. Ed.*, 2018, **57**, 12043–12047.

21 N. O. Moussa, G. Molnár, S. Bonhommeau, A. Zwick, S. Mouri, K. Tanaka, J. A. Real and A. Bousseksou, *Phys. Rev. Lett.*, 2005, **94**, 107205.

22 T. Matsumoto, G. N. Newton, T. Shiga, S. Hayami, Y. Matsui, H. Okamoto, R. Kumai, Y. Murakami and H. Oshio, *Nat. Commun.*, 2014, **5**, 3865.

23 M. Arczyński, J. Stanek, B. Sieklucka, K. R. Dunbar and D. Pinkowicz, *J. Am. Chem. Soc.*, 2019, **141**, 19067–19077.

24 J.-P. Launay and M. Verdaguer, *Electrons in Molecules: From Basic Principles to Molecular Electronics*, Oxford University Press, 2014.

25 J. Long, L.-M. Chamoreau, C. Mathonière and V. Marvaud, *Inorg. Chem.*, 2009, **48**, 22–24.

26 T. Korzeniak, S. Sasmal, D. Pinkowicz, W. Nitek, R. Pełka, D. Czernia, O. Stefańczyk and B. Sieklucka, *Inorg. Chem.*, 2020, **59**, 5872–5882.

27 M. Magott, O. Stefańczyk, B. Sieklucka and D. Pinkowicz, *Angew. Chem., Int. Ed.*, 2017, **56**, 13283–13287.

28 T. Liu, Y.-J. Zhang, S. Kanegawa and O. Sato, *J. Am. Chem. Soc.*, 2010, **132**, 8250–8251.

29 R. Ababei, C. Pichon, O. Roubeau, Y.-G. Li, N. Bréfuel, L. Buisson, P. Guionneau, C. Mathonière and R. Clérac, *J. Am. Chem. Soc.*, 2013, **135**, 14840–14853.

30 T. Liu, H. Zheng, S. Kang, Y. Shiota, S. Hayami, M. Mito, O. Sato, K. Yoshizawa, S. Kanegawa and C. Duan, *Nat. Commun.*, 2013, **4**, 2826.

31 M. Hojorat, H. Al Sabea, L. Norel, K. Bernot, T. Roisnel, F. Gendron, B. L. Guennic, E. Trzop, E. Collet, J. R. Long and S. Rigaut, *J. Am. Chem. Soc.*, 2020, **142**, 931–936.

32 Y.-J. Ma, J.-X. Hu, S.-D. Han, J. Pan, J.-H. Li and G.-M. Wang, *J. Am. Chem. Soc.*, 2020, **142**, 2682–2689.

33 G. Handzlik, M. Magott, B. Sieklucka and D. Pinkowicz, *Eur. J. Inorg. Chem.*, 2016, **2016**, 4872–4877.

34 D. Matoga, J. Szklarzewicz and M. Mikuriya, *Inorg. Chem.*, 2006, **45**, 7100–7104.

35 D. Wang, W. E. Crowe, R. M. Strongin and M. Sibrian-Vazquez, *Chem. Commun.*, 2009, 1876–1878.

36 J. Jia, A. J. Blake, N. R. Champness, P. Hubberstey, C. Wilson and M. Schröder, *Inorg. Chem.*, 2008, **47**, 8652–8664.

37 A. K. Cheetham, C. N. R. Rao and R. K. Feller, *Chem. Commun.*, 2006, 4780–4795.

38 P. Alemany, D. Casanova, S. Alvarez, C. Dryzun and D. Avnir, in *Reviews in Computational Chemistry*, 2017, pp. 289–352.

39 R. Podgajny, D. Pinkowicz, B. Czarnecki, M. Kozieł, S. Chorąży, M. Wis, W. Nitek, M. Rams and B. Sieklucka, *Cryst. Growth Des.*, 2014, **14**, 4030–4040.

40 E. Kuzniak-Glanowska, J. Kobylarczyk, K. Jedrzejowska, D. Glosz and R. Podgajny, *Dalton Trans.*, 2021, **50**, 10999–11015.

41 J. J. Borrás-Almenar, J. M. Clemente-Juan, E. Coronado and B. S. Tsukerblat, *J. Comput. Chem.*, 2001, **22**, 985–991.

42 M. Yuan, S. Gao, F. Zhao, W. Zhang and Z. Wang, *Sci. China, Ser. B: Chem.*, 2009, **52**, 266–275.

43 D. Pinkowicz, M. Rams, W. Nitek, B. Czarnecki and B. Sieklucka, *Chem. Commun.*, 2012, **48**, 8323–8325.

44 R. Boča, *Coord. Chem. Rev.*, 2004, **248**, 757–815.

45 A. Ozarowski, S. A. Zvyagin, W. M. Reiff, J. Telser, L.-C. Brunel and J. Krzystek, *J. Am. Chem. Soc.*, 2004, **126**, 6574–6575.

46 G. Novitchi, S. Jiang, S. Shova, F. Rida, I. Hlavička, M. Orlita, W. Wernsdorfer, R. Hamze, C. Martins, N. Suaud, N. Guihéry, A.-L. Barra and C. Train, *Inorg. Chem.*, 2017, **56**, 14809–14822.

47 C. Rojas-Dotti, N. Moliner, R. González and J. Martínez-Lillo, *J. Coord. Chem.*, 2018, **71**, 737–747.

48 R. L. Carlin, *Magnetochemistry*, Springer, Berlin, Heidelberg, 1986.

49 N. Bridonneau, J. Long, J. L. Cantin, J. von Bardeleben, S. Pillet, E. E. Bendeif, D. Aravena, E. Ruiz and V. Marvaud, *Chem. Commun.*, 2015, **51**, 8229–8232.

50 T. Korzeniak, R. Jankowski, M. Kozieł, D. Pinkowicz and B. Sieklucka, *Inorg. Chem.*, 2017, **56**, 12914–12919.

51 M. Magott, M. Sarewicz, S. Buda and D. Pinkowicz, *Inorg. Chem.*, 2020, **59**, 8925–8934.

52 X. Qi, P. Guionneau, E. Lafon, S. Perot, B. Kauffmann and C. Mathonière, *Magnetochemistry*, 2021, **7**, 97.

53 X. Qi, S. Pillet, C. de Graaf, M. Magott, E.-E. Bendeif, P. Guionneau, M. Rouzières, V. Marvaud, O. Stefańczyk, D. Pinkowicz and C. Mathonière, *Angew. Chem., Int. Ed.*, 2020, **59**, 3117–3121.

54 M. F. A. Hendrickx, V. S. Mironov, L. F. Chibotaru and A. Ceulemans, *Inorg. Chem.*, 2004, **43**, 3142–3150.

55 M. Magott, M. Reczyński, B. Gaweł, B. Sieklucka and D. Pinkowicz, *J. Am. Chem. Soc.*, 2018, **140**, 15876–15882.

56 M. Magott, B. Gaweł, M. Sarewicz, M. Reczyński, K. Ogorzały, W. Makowski and D. Pinkowicz, *Chem. Sci.*, 2021, **12**, 9176–9188.